

Resilient Practical Test-Time Adaptation: Soft Batch Normalization Alignment and Entropy-driven Memory Bank

Xingzhi Zhou^{1,3*}, Zhiliang Tian^{2†}, Ka Chun Cheung³, Simon See³, Nevin L. Zhang¹

¹Department of Computer Science and Engineering, HKUST

² College of Computer, NUDT

³NVIDIA AI Technology Center, NVIDIA

xingzhi.zhou@connect.ust.hk, tianzhiliang@nudt.edu.cn, {chcheung,ssee}@nvidia.com, lzhang@cse.ust.hk

Abstract

Test-time domain adaptation effectively adjusts the source domain model to accommodate unseen domain shifts in a target domain during inference. However, the model performance can be significantly impaired by continuous distribution changes in the target domain and non-independent and identically distributed (non-i.i.d.) test samples often encountered in practical scenarios. While existing memory bank methodologies use memory to store samples and mitigate non-i.i.d. effects, they do not inherently prevent potential model degradation. To address this issue, we propose a resilient practical test-time adaptation (ResiTTA) method focused on parameter resilience and data quality. Specifically, we develop a resilient batch normalization with estimation on normalization statistics and soft alignments to mitigate overfitting and model degradation. We use an entropy-driven memory bank that accounts for timeliness, the persistence of over-confident samples, and sample uncertainty for high-quality data in adaptation. Our framework periodically adapts the source domain model using a teacher-student model through a self-training loss on the memory samples, incorporating soft alignment losses on batch normalization. We empirically validate ResiTTA across various benchmark datasets, demonstrating state-of-the-art performance.

1 Introduction

Test-time domain adaptation (TTA) updates a source-pretrained model to a target domain during the inference stage by adjusting parameters using only unlabeled test data streams. Due to the domain shift between source training data and target test data, domain adaptation is essential for achieving superior performance. This makes TTA crucial for the practical deployment of machine perception applications confronting domain shifts. For instance, a semantic segmentation model trained on a dataset in clear weather conditions

performs poorly in rainy conditions [Colomer *et al.*, 2023]. Similarly, a pre-trained image classification model might experience degraded performance when tested on corrupted images generated from sensor-degraded cameras.

Continuous distribution changes in the target domain and temporal correlation present significant challenges in practical model deployment, particularly for traditional TTA methods that assume test samples are sampled from a fixed target domain distribution. These continuous distribution changes require a TTA method to adjust parameters dynamically and prevent catastrophic forgetting. The temporal correlation contributes to non-independent and identically distributed (non-i.i.d.) test samples, where test samples from certain classes may predominate in specific time slots.

Early TTA approaches have employed entropy minimization [Wang *et al.*, 2021] and pseudo-labels [Lee and others, 2013] to adjust the model to target domains. However, these strategies might overfit to particular domains, resulting in model performance decline when the distribution continuously changes in the target domain. CoTTA [Wang *et al.*, 2022] addresses continuous distribution changes. It utilizes a teacher-student model combined with augmentation-average methods to generate pseudo labels and stochastic parameter restoration to reduce overfitting. Nonetheless, CoTTA faces challenges with non-independent and identically distributed (non-i.i.d.) test samples during inference, as it is designed under the assumption of i.i.d. [Gong *et al.*, 2022; Yuan *et al.*, 2023]. NOTE [Gong *et al.*, 2022] introduces a memory bank strategy to handle the non-i.i.d. effect observed in inference with instance-aware batch normalization. This method suggests a balance between individual instance statistics and source statistics within batch normalization. However, instance statistics can be quite unstable, resulting in model degradation. RoTTA [Yuan *et al.*, 2023] enhances the memory bank approach by accounting for sample timeliness and uncertainty, and it stabilizes batch normalization statistics by continually updating global statistics with test-batch statistics. Still, existing memory-bank techniques do not fully address potential model degradation caused by overfitting on test samples in the target domain.

In this paper, to tackle potential model degradation, we propose a resilient practical test-time adaptation (ResiTTA) method. This method consists of three parts: resilient batch normalization, entropy-driven memory bank, and self-

*This work was done while Xingzhi was an intern at NVIDIA

†Corresponding Author

training adaptation. Resilient Batch Normalization (ResiBN), involves maintaining global target statistics for batch normalization. We update these statistics using an exponential moving average based on test-batch statistics. To prevent parameter overfitting, ResiBN employs soft alignments on the target statistics by minimizing the Wasserstein distance between the target statistics and the source statistics, where the source statistics are global statistics in batch normalization acquired during the source model training. Entropy-driven Memory Bank (EntroBank), updates samples by considering three factors: timeliness, the persistence of over-confident samples, and sample uncertainty to ensure high data quality. Timeliness addresses the issue of outdated samples that remained in the memory for too long. The persistence of over-confident samples refers to low-entropy samples over an extended period. Sample uncertainty is measured using the entropy of the predicted distribution as a metric for memory updates. In the adaptation stage, we periodically adapt the source pre-trained model using a teacher-student approach with samples from EntroBank via a self-training loss, coupled with soft alignment losses in batch normalization statistics. Our contributions are as follows:

- We propose a resilient practical test-time adaptation approach (ResiTTA) to counter potential model degradation under continuous distribution changes in the target domain and temporal correlation.
- To reduce parameter overfitting, we propose Resilient Batch Normalization which includes gradually updated target statistics in batch normalization and employs soft alignments on these statistics.
- To enhance data quality, we propose Entropy-Driven Memory Bank that considers the timeliness of data, the persistence of over-confident samples, and sample uncertainty.
- We conduct comprehensive experiments to validate ResiTTA on several common TTA benchmarks such as CIFAR10-C, CIFAR100-C, and ImageNet-C, where ResiTTA outperforms existing state-of-the-art results.

2 Related Works

2.1 Domain Adaptation

Domain adaptation (DA) concentrates on transferring knowledge from a source domain to a target domain [Tzeng *et al.*, 2015; Ganin *et al.*, 2016; Tsai *et al.*, 2018; Li *et al.*, 2021]. It falls into two categories: supervised and unsupervised, determined by the labeling status of the target domain data. The key approaches in DA includes latent distribution alignments [Long *et al.*, 2019; Xu *et al.*, 2019], adversarial training [Ganin *et al.*, 2016; Saito *et al.*, 2018], self-training [Zou *et al.*, 2018; Xie *et al.*, 2023], etc. Traditional DA techniques require access to both labeled source datasets and target datasets during training, which may limit their practical use when target domain data is unavailable. This limitation has spurred interest in test-time domain adaptation.

2.2 Test-Time Domain Adaptation

Test-time domain adaptation (TTA) aims to improve model performance at test time by adapting the model to the target domain distribution, utilizing only the source model and unlabeled target data [Chi *et al.*, 2021; Liu *et al.*, 2021; Qiu *et al.*, 2021; Chen *et al.*, 2022; Jang and Chung, 2023; Niu *et al.*, 2023]. TTA is categorized into offline and online settings. The offline setting allows the model to access all test samples, whereas the online setting processes test data in batches, more practical for real-world deployment. [Schneider *et al.*, 2020] demonstrates that building batch normalization statistics at test time significantly improves performance under domain shifts. TENT [Wang *et al.*, 2021] illustrates that adjusting batch normalization parameters with entropy minimization is effective for single target domain adaptation. EATA [Niu *et al.*, 2022] expands on this concept by incorporating weighted entropy minimization that accounts for reliability and diversity. It further applies elastic weight consolidation [Kirkpatrick *et al.*, 2017] from the continual learning field to mitigate catastrophic forgetting in the source domain.

Traditional TTA assumes test data is sampled from a fixed target domain. However, the target domain often experiences continuous distribution shifts in real-world scenarios. CoTTA [Wang *et al.*, 2022] addresses this challenge in TTA, termed continual test-time adaptation (CTTA). It employs a teacher-student model with augmentation-average pseudo labels and stochastic weight recovery to reduce overfitting. RMT [Döbler *et al.*, 2023] employs symmetric cross-entropy and contrastive learning for robust training. LAME [Boudiaf *et al.*, 2022], NOTE [Gong *et al.*, 2022], and RoTTA [Yuan *et al.*, 2023] tackle temporal correlation in TTA. LAME [Boudiaf *et al.*, 2022] fixes the source pre-trained model and modifies prediction probabilities by imposing a Laplacian constraint on the test batch. NOTE [Gong *et al.*, 2022] employs a memory bank to manage non-i.i.d. test samples and introduces instance-aware batch normalization for adaptation. RoTTA [Yuan *et al.*, 2023] handles both continuous distribution changes and temporal correlation in the target domain, forming the new problem setup practical test-time adaptation (PTTA). It uses a memory bank considering timeliness, category balance, and sample uncertainty. It also maintains global statistics in batch normalization continually updated with test-batch statistics. Nevertheless, existing memory bank methods may not fully address model degradation under simultaneous temporal correlation and continuous distribution changes. In this work, we introduce ResiTTA to tackle potential model degradation.

3 Method

3.1 Problem Definition

We adhere to the problem setup in practical test time adaptation (PTTA) [Yuan *et al.*, 2023]. Given a source pre-trained model f_{θ_s} with parameter θ_s pre-trained on the source domain dataset $\mathcal{D}_s = \{(x_s, y_s)\}$, the objective is to adapt f_{θ_s} to a sequence of online unlabeled samples $\mathcal{X}_1, \mathcal{X}_2, \dots, \mathcal{X}_T$. Each \mathcal{X}_t represents a batch of temporally correlated samples from a continuously evolving distribution \mathcal{P}_t . The goal is to make

inference $f_{\theta_t}(\mathcal{X}_t)$ using the adapted parameter θ_t at each time t .

3.2 Resilient Practical Test Time Adaptation

Motivated by the need to protect current models against potential deterioration due to continuous distribution changes in the target domain and temporal correlation, we develop resilient batch normalization (ResiBN) by gradually updating global target statistics and employing soft alignments by minimizing the Wasserstein distance between target statistics and source statistics. To get high-quality data for effective adaptation, we introduce an entropy-driven memory bank (EntroBank) factoring in timeliness, the persistence of over-confident samples, and sample uncertainty. In the adaptation stage, we employ a teacher-student method to periodically adapt the model to the target domain using memory samples through a self-training loss, complemented with soft alignment losses on the target statistics. We discuss ResiBN in sec. 3.3, EntroBank in sec. 3.4 and adaptation using a teacher-student model in sec. 3.5. The framework overview of ResiTTA is presented in Fig. 1.

3.3 Resilient Batch Normalization

Resilient Batch Normalization (ResiBN) maintains global target statistics μ_t, σ_t^2 , which are gradually updated by the test batch statistics in the batch normalization. Concurrently, ResiBN employs soft alignments on these target statistics by minimizing the Wasserstein distance between $\mathcal{N}(\mu_t, \sigma_t^2), \mathcal{N}(\mu_s, \sigma_s^2)$, where (μ_s, σ_s^2) denote the source statistics acquired in batch normalization during the source training stage.

In a 2-D batch normalization (BN) scenario with a given feature map $\mathbf{X} \in \mathbb{R}^{B \times C \times H \times W}$, the BN calculates mean $\mu \in \mathbb{R}^C$ and variance $\sigma^2 \in \mathbb{R}^C$ across B, H, W axes.

$$\mu_c = \frac{1}{BHW} \sum_{b=1}^B \sum_{h=1}^H \sum_{w=1}^W \mathbf{X}_{(b,c,h,w)}, \quad (1)$$

$$\sigma_c^2 = \frac{1}{BHW} \sum_{b=1}^B \sum_{h=1}^H \sum_{w=1}^W (\mathbf{X}_{(b,c,h,w)} - \mu_c)^2. \quad (2)$$

Subsequently, the feature map undergoes channel-wise normalization:

$$BN(\mathbf{X}_{(b,c,h,w)}; \mu, \sigma^2) = \gamma_c \frac{\mathbf{X}_{(b,c,h,w)} - \mu_c}{\sqrt{\sigma_c^2 + \epsilon}} + \beta_c, \quad (3)$$

where $\gamma, \beta \in \mathbb{R}^C$ are learnable affine parameters post-normalization, enhancing learning ability in the BN layer. ϵ is a small constant for numerical stability. In training, BN maintains global running mean and variance values (μ_s, σ_s^2) , termed source statistics in BN, measured by the exponential moving average of training batch statistics.

ResiBN maintains global target statistics μ_t, σ_t in batch normalization to stably estimate statistics amidst continual distribution changes and temporal correlation, following [Yuan *et al.*, 2023], μ_t, σ_t are updated by the test batch statistics:

$$\mu_t = (1 - \nu_b)\mu_t + \nu_b\mu_b, \quad (4)$$

$$\sigma_t^2 = (1 - \nu_b)\sigma_t^2 + \nu_b\sigma_b^2, \quad (5)$$

where μ_b, σ_b^2 are the test batch statistics. ν_b is the parameter controlling the update rate.

Continuous distribution changes in the target domain might lead to overfitting on the target statistics μ_t, σ_t . To enhance parameter resilience, we introduce a regularization of the target statistics inspired by continual learning [Kirkpatrick *et al.*, 2017]. We consider various divergence measures between source and target distribution, such as KL and JS divergence. However, we choose to minimize the Wasserstein distance [Villani and others, 2009] for numerical stability in BN. The reasoning for this choice over KL and JS divergence for soft alignments is elaborated in the appendix.

Soft alignments on the target statistics are achieved by minimizing Wasserstein distance:

$$\begin{aligned} \min W_2^2(\mathcal{N}(\mu_t, \sigma_t^2), \mathcal{N}(\mu_s, \sigma_s^2)) \\ = (\mu_s - \mu_t)^2 + \sigma_s^2 + \sigma_t^2 - 2\sigma_s\sigma_t. \end{aligned} \quad (6)$$

The derivative with respect to μ_t and σ_t^2 are:

$$\frac{dW_2^2}{d\mu_t} = 2(\mu_t - \mu_s), \quad (7)$$

$$\frac{dW_2^2}{d\sigma_t^2} = 1 - \frac{\sigma_s}{\sigma_t}. \quad (8)$$

Given that σ_t appears in the denominator in Eq. 8, which could cause numerical instability. We use the derivative with respect to σ_t :

$$\frac{dW_2^2}{d\sigma_t} = 2\sigma_t - 2\sigma_s. \quad (9)$$

Finally, μ_t, σ_t are updated for soft alignment with the source statistics as follows:

$$\mu_t = \mu_t - \eta_t \frac{dW_2^2}{d\mu_t}, \quad (10)$$

$$\sigma_t = \sigma_t - \eta_t \frac{dW_2^2}{d\sigma_t}, \quad (11)$$

where η_t denotes hyperparameters indicating the extent of regularization.

3.4 Entropy-driven Memory Bank

Entropy-driven Memory Bank (EntroBank) focuses on three aspects: timeliness, the persistence of over-confident samples, and sample uncertainty. Due to continual distribution changes, our priority is to remove outdated samples for timeliness. We then prioritize the removal of long-persisted over-confident samples to avoid overfitting. In the absence of outdated or long-persisted over-confident samples, we determine sample removal based on a comparison of sample uncertainty measured by entropy.

We mathematically describe EntroBank as follows. Assume the capacity of EntropyBank is N . We record a sample as (x, \hat{y}, α, e) , representing the sample, inferred label, age, and entropy. The inferred label \hat{y} is obtained by

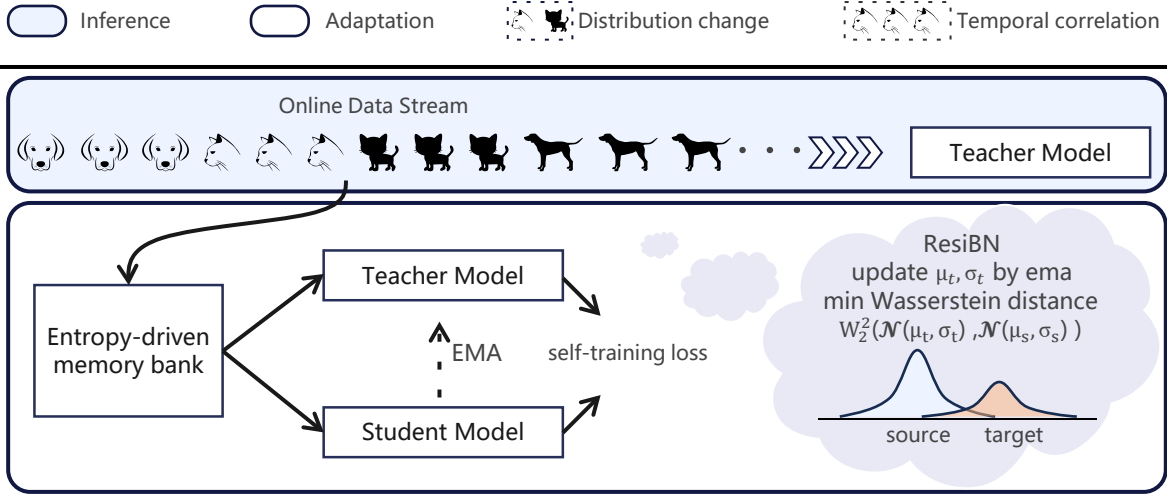


Figure 1: **Framework Overview.** We duplicate the pre-trained model into a student and a teacher model at the beginning of the test and replace the batch normalization layer with resilient batch normalization (ResiBN). In the inference stage, we use the teacher model to predict labels. In the adaptation stage, we collect online test streams by entropy-drive memory bank (EntroBank). We periodically adapt the model through a self-training loss on data drawn from the memory bank, incorporating soft alignment losses.

$\arg \max p(y|x) = \text{softmax}(f_{\theta^T}(x))$. The age of a sample starts at 0 and increases over time. The entropy e is calculated as $\sum_y -p(y|x) \log p(y|x)$.

When adding a new sample (x, \hat{y}, α, e) to EntroBank, if memory usage is below capacity, we directly add the sample. Otherwise, we apply removal strategies in this order: outdated samples, long-persisted over-confident samples, and sample uncertainty.

Considering categorical balance, we make replacements only in dominant classes \mathcal{D}_c , defined as classes with the highest sample count based on inferred labels:

$$\mathcal{D}_c = \{c | m[c] = \max_{i \in [C]} m[i]\}, \quad (12)$$

where $m[c]$ is the count for each class c indicated by inferred labels $\{\hat{y}\}$, and $[C]$ is the a set of class indices $1, 2, 3, \dots, C$.

For timeliness, we define outdated samples as those whose age α exceeds \mathcal{T}_{forget} , a hyperparameter:

$$\mathcal{X}_{od} = \{(x, \hat{y}, \alpha, e) | \alpha \geq \mathcal{T}_{forget}\}. \quad (13)$$

We identify outdated samples \mathcal{X}_{od} among the dominated classes \mathcal{D}_c . If \mathcal{X}_{od} is not empty, we remove a sample from \mathcal{X}_{od} with the largest age. If \mathcal{X}_{od} is empty, we consider long-persisted over-confident samples.

We define long-persisted over-confident samples as those whose age α exceeds \mathcal{T}_{mature} and have the smallest entropy e among their class in terms of inferred labels.

$$\mathcal{X}_{oc} = \{(x, \hat{y}, \alpha, e) | \alpha \geq \mathcal{T}_{mature}, e = \min_{\{i | i \in [N], \hat{y}_i = \hat{y}\}} e_i\}, \quad (14)$$

where $[N]$ is a set of samples indices in EntroBank $1, 2, 3, \dots, N$. If \mathcal{X}_{oc} is not empty, we remove a sample from \mathcal{X}_{oc} with the lowest entropy. If \mathcal{X}_{oc} is empty, we consider sample uncertainty.

We first define the sample $(x', \hat{y}', \alpha', e')$ with the highest entropy among the dominated classes \mathcal{D}_c . If $e < e'$, indicating lower uncertainty, we replace $(x', \hat{y}', \alpha', e')$ with the new

sample. Otherwise, we discard the new sample. The details of the sample adding in EntroBank are outlined in Algorithm 1.

Algorithm 1 EntroBank for sample adding

Input: sample x and the adapted model $f_{\theta'}$

Define: dominant classes \mathcal{D}_c , outdated samples: \mathcal{X}_{od} , long-existed over-confident samples: \mathcal{X}_{oc} .

- 1: Increase the age for each sample in memory
 - 2: Infer distribution: $p(y|x) = \text{softmax}(f_{\theta'}(x))$
 - 3: Predicted label: $\hat{y} = \arg \max p(y|x)$
 - 4: Initialize age: $\alpha = 0$
 - 5: Calculate entropy: $e = \sum_y -p(y|x) \log p(y|x)$
 - 6: **if** memory usage < capacity **then**
 - 7: Add (x, \hat{y}, α, e) to memory
 - 8: **else**
 - 9: Find \mathcal{D}_c by Eq. 12
 - 10: Find \mathcal{X}_{od} by Eq. 13 among \mathcal{D}_c
 - 11: Find \mathcal{X}_{oc} by Eq. 14 among \mathcal{D}_c
 - 12: Find sample x' with highest entropy e' among \mathcal{D}_c
 - 13: **if** \mathcal{X}_{od} is not \emptyset **then**
 - 14: Remove a sample $\in \mathcal{X}_{od}$ with the largest age
 - 15: Add (x, \hat{y}, α, e) to memory
 - 16: **else if** \mathcal{X}_{oc} is not \emptyset **then**
 - 17: Remove a sample $\in \mathcal{X}_{oc}$ with the lowest entropy
 - 18: Add (x, \hat{y}, α, e) to memory
 - 19: **else**
 - 20: **if** $e < e'$ **then**
 - 21: Remove the item containing x'
 - 22: Add (x, \hat{y}, α, e) to memory
 - 23: **else**
 - 24: Discard x
 - 25: **end if**
 - 26: **end if**
 - 27: **end if**
-

3.5 Self-Training Adapatation

In the adaptation phase, following the self-training method described in [Wang *et al.*, 2022], we employ a teacher-student model to adapt the source model using a self-training loss. The source pre-trained model is duplicated into a teacher model $f_{\theta'}$ and a student model f_{θ} . At time-step t , we first update the student model parameters from θ_t to θ_{t+1} using a self-training loss \mathcal{L}_s . This loss applies a strong augmentation view for the student model’s input and a weak augmentation view for the teacher model’s input ¹:

$$\mathcal{L}_s = \frac{1}{B} \sum_{i \in [B]} CE(p(\hat{y}|\mathcal{T}_w(x), \theta'_t), p(\hat{y}|\mathcal{T}_s(x), \theta_t)), \quad (15)$$

where $CE(\cdot, \cdot)$ represents the cross entropy operation, defined as $CE(p, q) = -\sum p \log q$. Samples $\{x\}$ are drawn from the memory bank, with B denoting the occupation of the memory bank. $\mathcal{T}_s, \mathcal{T}_w$ denote strong and weak augmentations respectively. $p(\hat{y}|\mathcal{T}_w(x), \theta'_t) = \text{softmax}(f_{\theta'_t}(\mathcal{T}_w(x)))$, where θ'_t refers to the parameters of the teacher model at time step t . $p(\hat{y}|\mathcal{T}_s(x), \theta_t) = \text{softmax}(f_{\theta_t}(\mathcal{T}_s(x)))$, where θ_t refers to the parameters of the student model at time step t .

The teacher model is updated using an exponential moving average of the parameters of the student model:

$$\theta'_{t+1} = (1 - \nu_m)\theta'_t + \nu\theta_{t+1}, \quad (16)$$

where ν_m is a parameter controlling the update rate in the teacher model.

In summary, we utilize EntroBank to manage sample storage within capacity constraints and replace batch normalization with ResiBN. We periodically adapt the source pre-trained model through a self-training approach on the memory samples, incorporating a soft alignment loss on batch normalization.

4 Experiments

In this section, we design experiments to compare ResiTtA with state-of-the-art (SOTA) methods under practical test-time adaptation (PTTA) setting [Yuan *et al.*, 2023] on CIFAR10-C, CIFAR100-C, and ImageNet-C [Hendrycks and Dietterich, 2019]. We then conduct ablation studies of ResiTtA on CIFAR100-C to demonstrate the effectiveness of each module design. Finally, we perform parameter analysis on the parameters $\eta_t, \mathcal{T}_{forget}$ and \mathcal{T}_{mature} .

4.1 Datasets

We validate our method on CIFAR10C, CIFAR100-C, and ImageNet-C, which are benchmarks created by [Hendrycks and Dietterich, 2019]. CIFAR10-C and CIFAR100-C are corruption versions of CIFAR10 and CIFAR100 [Krizhevsky *et al.*, 2009], featuring 15 types of corruption, each with 5 different degrees of severity. Each type and degree of corruption in CIFAR10-C and CIFAR100-C contains 10,000 samples,

¹We adhere to the augmentation practices from prior research [Wang *et al.*, 2022; Yuan *et al.*, 2023], utilizing ReSize+CenterCrop for the weak augmentation view, and ColorJitter + RandomAffine + RandomHorizontalFlip + GaussianBlur + GaussianNoise as the main augmentations for the strong augmentation view.

falling into 10 and 100 classes, respectively. ImageNet-C is a corruption version of the ImageNet [Deng *et al.*, 2009] validation dataset, with 15 types of corruption and 5 different degrees of severity. Each type and degree of corruption in ImageNet-C contains 5,000 samples falling into 1,000 classes.

4.2 Baselines

We compare our method with the following test-time adaptation algorithms: 1) **Source**: This approach infers test-time samples using the pre-trained model without any adaptation updates; 2) Prediction time batch normalization (**BN**) [Nado *et al.*, 2020]: This method freezes the pre-trained model weights and infers test-time samples by using the batch norm statistics from the test batch; 3) Pseudo-labeling (**PL**) [Lee and others, 2013]: This technique generates pseudo labels using the inferred labels and updates models using the cross entropy on the pseudo labels; 4) **TENT** [Wang *et al.*, 2021]: This method aims to adapt model by minimizing the entropy of predictions on test data to reduce generalization error; 5) **LAME** [Boudiaf *et al.*, 2022]: This approach fixes the pre-trained model but adjusts the output probability by adding Laplacian constraints to the local batch; 6) **CoTTA** [Wang *et al.*, 2022]: This algorithm uses a teacher-student model with an average augmentation strategy and stochastic weight recovery; 7) **NOTE** [Gong *et al.*, 2022]: This method employs an instance-aware batch normalization and a category-balanced memory bank. 8) **RoTTA** [Yuan *et al.*, 2023]: This method maintains global batch norm statistics with exponential average updates on test-batch statistics and a class-balanced memory bank considering uncertainty and timeliness. RoTTA adapts the pre-trained model by a timeliness-aware adaptation loss with a teacher-student model.

4.3 Implementation Details

We follow the model selection criteria of previous methods [Wang *et al.*, 2022; Yuan *et al.*, 2023] from the Robust-Bench benchmark [Croce *et al.*, 2021], using WildResNet-28 [Zagoruyko and Komodakis, 2016] for CIFAR10 → CIFAR10-C, ResNeXt-29 [Xie *et al.*, 2017] for CIFAR100 → CIFAR100-C and the standard resnet50 from [Croce *et al.*, 2021] for ImageNet → ImageNet-C. Consistent with the dataset protocol in [Yuan *et al.*, 2023], we simulate continuous distribution changes by altering the test domain at severity level 5 and use Dirichlet distribution sampling to model a non i.i.d. test stream for CIFAR10-C/100-C. Due to the limited number of samples per class in ImageNet-C, Dirichlet sampling cannot form an effective temporal correlation. Following [Gong *et al.*, 2022], we sort ImageNet-C classes within each corruption type to mimic temporal correlation, with further details provided in the appendix. We use Adam as the optimizer with a learning rate of 1.0×10^{-3} and a beta value of 0.9. The batch size is set to 64. The memory bank capacity and the update frequency are also set to 64 for all memory bank approaches for a fair comparison. The parameters $\nu_m = 1.0 \times 10^{-3}$, $\nu_b = 0.05$, and $\delta = 0.1$ are chosen. We use η_t values of 0.01 for CIFAR10-C/100-C and 0.05 for ImageNet-C, with the larger η_t for ImageNet-C accounting

Table 1: Classification error rate (%) of the task CIFAR10 \rightarrow CIFAR10-C online continual test-time adaptation evaluated on WideResNet-28 at the largest corruption severity 5. Samples in each corruption are correlatively sampled under the setup PTTA.

Time	t															Avg.
	motion	snow	fog	shot	defocus	contrast	zoom	brightness	frost	elastic	glass	gaussian	pixelate	jpeg	impulse	
Source	34.8	25.1	26.0	65.7	46.9	46.7	42.0	9.3	41.3	26.6	54.3	72.3	58.5	30.3	72.9	43.5
BN [Nado <i>et al.</i> , 2020]	73.2	73.4	72.7	77.2	73.7	72.5	72.9	71.0	74.1	77.7	80.0	76.9	75.5	78.3	79.0	75.2
PL [Lee and others, 2013]	73.9	75.0	75.6	81.0	79.9	80.6	82.0	83.2	85.3	87.3	88.3	87.5	87.5	87.5	88.2	82.9
TENT [Wang <i>et al.</i> , 2021]	74.3	77.4	80.1	86.2	86.7	87.3	87.9	87.4	88.2	89.0	89.2	89.0	88.3	89.7	89.2	86.0
LAME [Boudiaf <i>et al.</i> , 2022]	29.5	19.0	20.3	65.3	42.4	43.4	36.8	5.4	37.2	18.6	51.2	73.2	57.0	22.6	71.3	39.5
CoTTA [Wang <i>et al.</i> , 2022]	77.1	80.6	83.1	84.4	83.9	84.2	83.1	82.6	84.4	84.2	84.5	84.6	82.7	83.8	84.9	83.2
NOTE [Gong <i>et al.</i> , 2022]	18.0	22.1	20.6	35.6	26.9	13.6	26.5	17.3	27.2	37.0	48.3	38.8	42.6	41.9	49.7	31.1
RoTTA [Yuan <i>et al.</i> , 2023]	18.1	21.3	<u>18.8</u>	<u>33.6</u>	23.6	<u>16.5</u>	<u>15.1</u>	11.2	<u>21.9</u>	<u>30.7</u>	<u>39.6</u>	<u>26.8</u>	<u>33.7</u>	<u>27.8</u>	<u>39.5</u>	<u>25.2</u>
ResiTTA	18.4	<u>19.5</u>	15.5	30.5	<u>23.8</u>	12.2	14.0	9.3	18.5	<u>24.6</u>	35.8	24.9	27.7	22.6	39.1	22.4

Table 2: Classification error rate (%) of the task CIFAR100 \rightarrow CIFAR100-C online continual test-time adaptation evaluated on the ResNeXt-29 architecture at the largest corruption severity 5. Samples in each corruption are correlatively sampled under the setup PTTA.

Time	t															Avg.
	motion	snow	fog	shot	defocus	contrast	zoom	brightness	frost	elastic	glass	gaussian	pixelate	jpeg	impulse	
Source	30.8	39.5	50.3	68.0	29.3	55.1	28.8	29.5	45.8	37.2	54.1	73.0	74.7	41.2	39.4	46.4
BN [Nado <i>et al.</i> , 2020]	48.5	54.0	58.9	56.2	46.4	48.0	47.0	45.4	52.9	53.4	57.1	58.2	51.7	57.1	58.8	52.9
PL [Lee and others, 2013]	50.6	62.1	73.9	87.8	90.8	96.0	94.8	96.4	97.4	97.2	97.4	97.4	97.3	97.4	97.4	88.9
TENT [Wang <i>et al.</i> , 2021]	53.3	77.6	93.0	96.5	96.7	97.5	97.1	97.5	97.3	97.2	97.1	97.7	97.6	98.0	98.3	92.8
LAME [Boudiaf <i>et al.</i> , 2022]	22.4	30.4	43.9	66.3	21.3	51.7	20.6	21.8	39.6	28.0	48.7	72.8	74.6	33.1	32.3	40.5
CoTTA [Wang <i>et al.</i> , 2022]	49.2	52.7	56.8	53.0	48.7	51.7	49.4	48.7	52.5	52.2	54.3	54.9	49.6	53.4	56.2	52.2
NOTE [Gong <i>et al.</i> , 2022]	45.7	53.0	58.2	65.6	54.2	52.0	59.8	63.5	74.8	91.8	98.1	98.3	96.8	97.0	98.2	73.8
RoTTA [Yuan <i>et al.</i> , 2023]	31.8	36.7	<u>40.9</u>	<u>42.1</u>	30.0	<u>33.6</u>	27.9	25.4	<u>32.3</u>	34.0	38.8	38.7	31.3	38.0	42.9	<u>35.0</u>
ResiTTA	<u>29.2</u>	<u>33.9</u>	39.5	39.4	<u>28.4</u>	29.2	<u>26.5</u>	<u>24.8</u>	30.8	<u>33.9</u>	37.5	38.6	<u>31.6</u>	<u>37.9</u>	41.5	33.5

for dataset complexity, which validated in our parameter analysis in sec. 4.6.

4.4 Main Results

CIFAR10 \rightarrow CIFAR10-C We report the classification error rate for the CIFAR-10-to-CIFAR10C task in Table 1. ResiTTA achieves the lowest average error value and outperforms other methods in 10 out of 15 corruption types. When compared to the best-performing baseline, RoTTA [Yuan *et al.*, 2023], our method reduces the average error rate from 25.2% to 22.4%. NOTE [Gong *et al.*, 2022] and RoTTA [Yuan *et al.*, 2023] obtain results comparable to ours for the initial corruption type, but they exhibit weaker performance on subsequent corruption types. This trend highlights the effectiveness of ResiBN in reducing parameter overfitting. Additionally, our method consistently matches or exceeds the Source model across all corruption types, indicating its ability to mitigate potential model degradation

CIFAR100 \rightarrow CIFAR100-C We report the performance of ResiTTA on the CIFAR100-to-CIFAR100-C task in Table 2. ResiTTA achieves the lowest average classification error, reducing the average error rate from 35.0% to 33.5% in comparison to the previously best-performing method, RoTTA [Yuan *et al.*, 2023]. LAME [Boudiaf *et al.*, 2022], a non-parametric approach, yields results comparable to ResiTTA and achieves the best performance in several corruption types. However, the performance of LAME varies significantly across corruption types, largely depending on the performance of the pre-trained model.

ImageNet \rightarrow ImageNet-C We report the results of all baselines and ResiTTA on the ImageNet-to-ImageNet-C task in Table 3. ResiTTA outperforms other methods in average classification error and achieves the best performance in 13

out of 15 corruption types. It reduces the average test error from 71.6% to 66.7% compared to RoTTA [Yuan *et al.*, 2023]. Specifically, in the corruption types *jpeg* and *impulse* among the last two domains, ResiTTA decreases the classification error from 58.8% to 53.6% and from 84.5% to 75.5% respectively, compared with the previous best results. These findings demonstrate the effectiveness ResiTTA in reducing overfitting and model degradation

4.5 Ablation Study

In Table 4, we present different model variants by replacing or removing components to validate the module effectiveness in ResiTTA in the CIFAR100-to-CIFAR100-C task. In row 2, We first replace ResiBN by prediction time batch normalization (BN) [Nado *et al.*, 2020], resulting in a significant increase in average test error from 33.5 % to 51.6 %, due to unstable batch-wise statistics. Substituting ResiBN with RBN [Yuan *et al.*, 2023] led to an increase in average error from 33.5 % to 35.4 % (row 3). RBN uses an exponential moving average update for target statistics during inference but does not address the potential for overfitting on the test batches. Next, we individually remove three strategies in EntroBank. Eliminating the strategy for outdated samples (row 4) raises the error rate to 33.9 %. Omitting the strategy for long-persisted over-confident samples increases the error rate to 35.4 % (row 5). Removing the strategy for sample uncertainty significantly elevated the error rate to 38.2 % (row 6). These results demonstrate the importance of the three strategies in EntroBank.

4.6 Parameter Analysis

In this section, we examine the sensitivity of hyperparameters: η_t , \mathcal{T}_{mature} , \mathcal{T}_{forget} by adjusting each parameter from the default setup. For each parameter, we calculate the aver-

Table 3: Classification error rate (%) of the task ImageNet \rightarrow ImageNet-C online continual test-time adaptation evaluated on the resnet50 architecture at the largest corruption severity 5. Samples in each corruption are correlatively arranged following [Gong *et al.*, 2022]

Time	t															Avg.
	motion	snow	fog	shot	defocus	contrast	zoom	brightness	frost	elastic	glass	gaussian	pixelate	jpeg	impulse	
Source	85.5	83.5	76.4	96.5	81.8	94.6	78.1	41.2	77.4	83.0	89.7	97.1	79.1	67.5	97.5	81.9
BN [Nado <i>et al.</i> , 2020]	86.0	80.8	71.1	90.4	92.4	90.4	79.0	58.4	81.9	75.5	92.4	90.7	71.1	76.2	90.6	81.8
PL [Lee and others, 2013]	87.2	88.3	86.4	97.2	98.9	99.6	99.1	98.5	99.6	99.6	99.7	99.8	99.7	99.7	99.7	96.9
TENT [Wang <i>et al.</i> , 2021]	84.9	78.9	69.4	87.9	89.4	87.6	79.1	64.4	83.0	77.2	91.2	88.9	78.0	80.4	89.6	82.0
LAME [Boudiaf <i>et al.</i> , 2022]	85.3	83.4	76.1	96.7	80.6	94.1	76.1	34.6	76.2	83.2	89.9	97.4	77.5	63.8	97.9	80.8
CoTTA [Wang <i>et al.</i> , 2022]	86.9	80.4	71.7	87.3	90.8	89.4	78.1	60.5	78.8	73.1	89.4	85.0	67.8	72.6	84.5	79.8
NOTE [Gong <i>et al.</i> , 2022]	83.9	79.6	78.2	93.5	97.3	94.4	96.7	92.1	97.1	98.1	99.3	99.4	98.6	98.9	99.6	93.8
RoTTA [Yuan <i>et al.</i> , 2023]	78.3	76.2	59.9	88.2	87.7	84.7	66.1	40.4	69.6	58.4	78.1	86.2	56.7	58.8	85.6	71.6
ResiTtA	74.4	69.2	54.0	82.9	<u>80.7</u>	75.8	63.9	<u>37.5</u>	65.6	57.2	76.8	77.5	55.7	53.6	75.5	66.7

Table 4: **Important component for ResiTtA.** Average classification error rate (%) of task CIFAR100 \rightarrow CIFAR100-C. For the different variants, we highlight the differences from the default ResiTtA setting.

Method	AdBN	RBN	ResiBN	\mathcal{X}_{od}	\mathcal{X}_{oc}	SU	CIFAR100C
1 ResiTtA	X	X	✓	✓	✓	✓	33.5
2	✓	X	X	✓	✓	✓	51.6
3	X	✓	X	✓	✓	✓	35.4
4	X	X	✓	X	✓	✓	33.9
5	X	X	✓	✓	X	✓	35.4
6	X	X	✓	✓	✓	X	38.2

\mathcal{X}_{od} : outdated samples, \mathcal{X}_{oc} : long-existed over-confident samples
 SU: sample uncertainty, ResiBN: Resilient Batch Norm
 BN: prediction time batch normalization [Nado *et al.*, 2020]
 RBN: robust Batch Norm [Yuan *et al.*, 2023]

age classification error across the CIFAR10-to-CIFAR10-C, the CIFAR100-to-CIFAR100-C, and ImageNet-to-ImageNet-C tasks over 15 corruptions types with severity 5 using the default corruption order and correlation sampling methods.

First, we investigate the parameter η_t in Table 5. This parameter determines the strength of soft alignments between source and target statistics in batch normalization. We vary η_t within [0.001, 0.005, 0.01, 0.05, 0.1]. For CIFAR10-C and CIFAR100-C, the optimal results occur at $\eta_t = 0.01$. Deviations from this value lead to performance decline. In contrast, the best result of ImageNet-C is achieved at $\eta_t = 0.05$, differing from CIFAR10-C/100-C due to the complexity of ImageNet and the large number of classes. This data complexity makes capturing batch normalization statistics in test time challenging and prone to overfitting. Consequently, ResiTtA requires stronger soft alignments of batch normalization statistics for the ImageNet-to-ImageNet-C task.

Table 5: **Parameter analysis on η_t .** Average classification error (%).

η_t	CIFAR10-C	CIFAR100-C	ImageNet-C
0.001	23.0	34.1	73.5
0.005	22.7	33.8	72.0
0.01	22.4	33.5	70.6
0.05	25.6	33.9	66.7
0.1	30.6	35.8	68.4

Next, we examine \mathcal{T}_{mature} in Table 6. This parameter regulates the duration low-entropy samples remain. Increasing \mathcal{T}_{mature} from 200 leads to a gradual increase in error rate across all datasets: from 22.4 % to 23.4 % on CIFAR10-C,

from 33.5 % to 34.9 % on CIFAR100-C, and 66.7 % to 67.8 % on ImageNet-C. This indicates that extending the existence of over-confident samples declines performance.

Table 6: **Parameter analysis on \mathcal{T}_{mature} .** Average classification error (%).

\mathcal{T}_{mature}	CIFAR10-C	CIFAR100-C	ImageNet-C
100	22.8	33.2	67.1
200	22.4	33.5	66.7
300	23.0	33.6	67.1
400	23.1	34.0	67.1
500	23.1	34.2	67.6
600	23.0	34.4	67.6
700	23.1	34.8	67.8
800	23.4	34.9	67.8

Lastly, we analyze \mathcal{T}_{forget} in Table 7. We find that ResiTtA is relatively insensitive to \mathcal{T}_{forget} . This is because a small proportion of samples become outdated. Most samples in the memory bank are updated in prediction probability $p(\hat{y}|x, \theta')$, resulting in a gradual decrease in entropy. Additionally, \mathcal{T}_{forget} being significantly larger than \mathcal{T}_{mature} means most samples are classified as long-persisted over-confident samples before being considered outdated.

Table 7: **Parameter analysis on \mathcal{T}_{forget} .** Average classification error (%).

\mathcal{T}_{forget}	CIFAR10-C	CIFAR100-C	ImageNet-C
500	22.6	33.6	66.9
1000	22.4	33.5	66.7
1500	22.2	33.7	67.1
2000	22.5	33.6	66.8
2500	22.4	33.8	66.9

5 Conclusion

Addressing potential model degradation in a practical test-time adaptation setting, we propose a resilient practical test-time adaptation (ResiTtA) method, which incorporates three parts: resilient batch normalization, entropy-driven memory bank, and self-training adaptation. Resilient batch normalization updates global target statistics progressively with test-batch statistics in batch normalization and implements soft alignment on these target statistics by minimizing to reduce parameter overfitting. The entropy-driven memory bank is developed to provide high-quality samples, considering three aspects: timeliness, the persistence of over-confident samples, and sample uncertainty. The model is adapted periodically by a teacher-student model using a self-training loss on

memory samples, incorporating soft alignment losses. Extensive experiments, ablation studies, and parameter analysis are conducted for validation of the effectiveness of ResiTTA.

References

- [Boudiaf *et al.*, 2022] Malik Boudiaf, Romain Mueller, Ismail Ben Ayed, and Luca Bertinetto. Parameter-free online test-time adaptation. In *CVPR*, pages 8344–8353, 2022.
- [Chen *et al.*, 2022] Dian Chen, Dequan Wang, Trevor Darrell, and Sayna Ebrahimi. Contrastive test-time adaptation. In *CVPR*, pages 295–305, 2022.
- [Chi *et al.*, 2021] Zhixiang Chi, Yang Wang, Yuanhao Yu, and Jin Tang. Test-time fast adaptation for dynamic scene deblurring via meta-auxiliary learning. In *CVPR*, pages 9137–9146, 2021.
- [Colomer *et al.*, 2023] Marc Botet Colomer, Pier Luigi Dovesi, Theodoros Panagiotakopoulos, Joao Frederico Carvalho, Linus Härenstam-Nielsen, Hossein Azizpour, Hedvig Kjellström, Daniel Cremers, and Matteo Poggi. To adapt or not to adapt? real-time adaptation for semantic segmentation. In *ICCV*, pages 16548–16559, 2023.
- [Croce *et al.*, 2021] Francesco Croce, Maksym Andriushchenko, Vikash Sehwal, Edoardo DeBenedetti, Nicolas Flammarion, Mung Chiang, Prateek Mittal, and Matthias Hein. Robustbench: a standardized adversarial robustness benchmark. In *NeurIPS*, 2021.
- [Deng *et al.*, 2009] Jia Deng, Wei Dong, Richard Socher, Li-Jia Li, Kai Li, and Li Feifei. Imagenet: A large-scale hierarchical image database. In *CVPR*, pages 248–255, 2009.
- [Döbler *et al.*, 2023] Mario Döbler, Robert A Marsden, and Bin Yang. Robust mean teacher for continual and gradual test-time adaptation. In *CVPR*, pages 7704–7714, 2023.
- [Ganin *et al.*, 2016] Yaroslav Ganin, Evgeniya Ustinova, Hana Ajakan, Pascal Germain, Hugo Larochelle, François Laviolette, Mario March, and Victor Lempitsky. Domain-adversarial training of neural networks. *Journal of Machine Learning Research*, 17(59):1–35, 2016.
- [Gong *et al.*, 2022] Taesik Gong, Jongheon Jeong, Taewon Kim, Yewon Kim, Jinwoo Shin, and Sung-Ju Lee. Robust continual test-time adaptation: Instance-aware BN and prediction-balanced memory. In *NeurIPS*, 2022.
- [Hendrycks and Dietterich, 2019] Dan Hendrycks and Thomas G. Dietterich. Benchmarking neural network robustness to common corruptions and perturbations. In *ICLR*, 2019.
- [Jang and Chung, 2023] Minguk Jang and Sae-Young Chung. Test-time adaptation via self-training with nearest neighbor information. In *ICLR*, 2023.
- [Kirkpatrick *et al.*, 2017] James Kirkpatrick, Razvan Pascanu, Neil Rabinowitz, Joel Veness, Guillaume Desjardins, Andrei A. Rusu, Kieran Milan, John Quan, Tiago Ramalho, Agnieszka Grabska-Barwinska, Demis Hassabis, Claudia Clopath, Dharshan Kumaran, and Raia Hadsell. Overcoming catastrophic forgetting in neural networks. *Proceedings of the National Academy of Sciences*, 114(13):3521–3526, 2017.
- [Krizhevsky *et al.*, 2009] Alex Krizhevsky, Geoffrey Hinton, et al. Learning multiple layers of features from tiny images. 2009.
- [Lee and others, 2013] Dong-Hyun Lee et al. Pseudo-label: The simple and efficient semi-supervised learning method for deep neural networks. In *Workshop on challenges in representation learning, ICML*, volume 3, page 896, 2013.
- [Li *et al.*, 2021] Shuang Li, Mixue Xie, Kaixiong Gong, Chi Harold Liu, Yulin Wang, and Wei Li. Transferable semantic augmentation for domain adaptation. In *CVPR*, pages 11516–11525, June 2021.
- [Liu *et al.*, 2021] Yuejiang Liu, Parth Kothari, Bastien van Delft, Baptiste Bellot-Gurlet, Taylor Mordan, and Alexandre Alahi. Ttt++: When does self-supervised test-time training fail or thrive? In *NeurIPS*, volume 34, 2021.
- [Long *et al.*, 2019] Mingsheng Long, Yue Cao, Zhangjie Cao, Jianmin Wang, and Michael I. Jordan. Transferable representation learning with deep adaptation networks. *IEEE Transactions on Pattern Analysis and Machine Intelligence*, 41(12):3071–3085, 2019.
- [Nado *et al.*, 2020] Zachary Nado, Shreyas Padhy, D Sculley, Alexander D’Amour, Balaji Lakshminarayanan, and Jasper Snoek. Evaluating prediction-time batch normalization for robustness under covariate shift. *arXiv preprint arXiv:2006.10963*, 2020.
- [Niu *et al.*, 2022] Shuaicheng Niu, Jiayang Wu, Yifan Zhang, Yafo Chen, Shijian Zheng, Peilin Zhao, and Mingkui Tan. Efficient test-time model adaptation without forgetting. In *ICML*, pages 16888–16905, 2022.
- [Niu *et al.*, 2023] Shuaicheng Niu, Jiayang Wu, Yifan Zhang, Zhiquan Wen, Yafo Chen, Peilin Zhao, and Mingkui Tan. Towards stable test-time adaptation in dynamic wild world. In *ICLR*, 2023.
- [Qiu *et al.*, 2021] Zhen Qiu, Yifan Zhang, Hongbin Lin, Shuaicheng Niu, Yanxia Liu, Qing Du, and Mingkui Tan. Source-free domain adaptation via avatar prototype generation and adaptation. In *IJCAI*, pages 2921–2927. International Joint Conferences on Artificial Intelligence Organization, 2021.
- [Saito *et al.*, 2018] Kuniaki Saito, Kohei Watanabe, Yoshitaka Ushiku, and Tatsuya Harada. Maximum classifier discrepancy for unsupervised domain adaptation. In *CVPR*, June 2018.
- [Schneider *et al.*, 2020] Steffen Schneider, Evgenia Rusak, Luisa Eck, Oliver Bringmann, Wieland Brendel, and Matthias Bethge. Improving robustness against common corruptions by covariate shift adaptation. In *NeurIPS*, 2020.
- [Tsai *et al.*, 2018] Yi-Hsuan Tsai, Wei-Chih Hung, Samuel Schulter, Kihyuk Sohn, Ming-Hsuan Yang, and Manmohan Chandraker. Learning to adapt structured output space for semantic segmentation. In *CVPR*, June 2018.

- [Tzeng *et al.*, 2015] Eric Tzeng, Judy Hoffman, Trevor Darrell, and Kate Saenko. Simultaneous deep transfer across domains and tasks. In *ICCV*, December 2015.
- [Villani and others, 2009] Cédric Villani et al. *Optimal transport: old and new*, volume 338. Springer, 2009.
- [Wang *et al.*, 2021] Dequan Wang, Evan Shelhamer, Shaoteng Liu, Bruno A. Olshausen, and Trevor Darrell. Tent: Fully test-time adaptation by entropy minimization. In *ICLR*, 2021.
- [Wang *et al.*, 2022] Qin Wang, Olga Fink, Luc Van Gool, and Dengxin Dai. Continual test-time domain adaptation. In *CVPR*, pages 7191–7201, 2022.
- [Xie *et al.*, 2017] Saining Xie, Ross Girshick, Piotr Dollár, Zhuowen Tu, and Kaiming He. Aggregated residual transformations for deep neural networks. In *CVPR*, pages 5987–5995, 2017.
- [Xie *et al.*, 2023] Binhui Xie, Shuang Li, Mingjia Li, Chi Harold Liu, Gao Huang, and Guoren Wang. Sepico: Semantic-guided pixel contrast for domain adaptive semantic segmentation. *IEEE Transactions on Pattern Analysis and Machine Intelligence*, 45(7):9004–9021, 2023.
- [Xu *et al.*, 2019] Ruijia Xu, Guanbin Li, Jihan Yang, and Liang Lin. Larger norm more transferable: An adaptive feature norm approach for unsupervised domain adaptation. In *ICCV*, October 2019.
- [Yuan *et al.*, 2023] Longhui Yuan, Binhui Xie, and Shuang Li. Robust test-time adaptation in dynamic scenarios. In *CVPR*, pages 15922–15932, 2023.
- [Zagoruyko and Komodakis, 2016] Sergey Zagoruyko and Nikos Komodakis. Wide residual networks. In *BMVC*, 2016.
- [Zou *et al.*, 2018] Yang Zou, Zhiding Yu, B.V.K. Vijaya Kumar, and Jinsong Wang. Unsupervised domain adaptation for semantic segmentation via class-balanced self-training. In *ECCV*, September 2018.

APPENDIX

In this appendix, we further explain the technical details of ResiTTA including divergence selection in sec. A, implementation details in sec. B, and extra experiment results in sec. C.

A Divergence Selection

In sec. 3.3, we choose Wasserstein distance for soft alignments on batch normalization statistics μ_t, σ_t , and we illustrate the reason why not using KL or JS divergences to maintain numerical stability.

We first obtain the KL divergence between source and target statistics:

$$KL(\mathcal{N}(\mu_t, \sigma_t^2), \mathcal{N}(\mu_s, \sigma_s^2)) = \frac{1}{2} \left(\frac{\sigma_t^2}{\sigma_s^2} + \frac{(\mu_t - \mu_s)^2}{\sigma_s^2} - 1 + 2 \ln \left(\frac{\sigma_s}{\sigma_t} \right) \right). \quad (17)$$

Taking derivative towards $\mu_t, \sigma_t^2, \sigma_t$, we have:

$$\frac{dKL(\cdot)}{d\mu_t} = \frac{(\mu_t - \mu_s)}{\sigma_s^2}, \quad (18)$$

$$\frac{dKL(\cdot)}{d\sigma_t^2} = \frac{1}{2\sigma_s^2} - \frac{1}{2\sigma_t^2}, \quad (19)$$

$$\frac{dKL(\cdot)}{d\sigma_t} = \frac{\sigma_t^2 - \sigma_s^2}{\sigma_t \sigma_s^2}. \quad (20)$$

$$(21)$$

We observe the denominators of all derivatives contain either σ_s or σ_t , contributing to numerical stability. We can obtain the same conclusion for the case $KL(\mathcal{N}(\mu_s, \sigma_s^2), \mathcal{N}(\mu_t, \sigma_t^2))$ using the same approach.

We now turn to JS divergence between source and target statistics:

$$JS(\mathcal{N}(\mu_t, \sigma_t^2), \mathcal{N}(\mu_s, \sigma_s^2)) = \frac{1}{4} \left(\frac{\sigma_t^2}{\sigma_s^2} + \frac{\sigma_s^2}{\sigma_t^2} + \left(\frac{1}{\sigma_s^2} + \frac{1}{\sigma_t^2} \right) (\mu_t - \mu_s)^2 - 2 \right). \quad (22)$$

We take derivatives towards $\mu_t, \sigma_t^2, \sigma_t$:

$$\frac{dJS(\cdot)}{d\mu_t} = \left(\frac{1}{2\sigma_s^2} + \frac{1}{2\sigma_t^2} \right) (\mu_t - \mu_s), \quad (23)$$

$$\frac{dJS(\cdot)}{d\sigma_t^2} = \frac{1}{4\sigma_s^2} - \frac{\sigma_s^2}{4\sigma_t^4} + \frac{(\mu_t - \mu_s)^2}{4\sigma_t^4}, \quad (24)$$

$$\frac{dJS(\cdot)}{d\sigma_t} = \frac{\sigma_t}{2\sigma_s^2} - \frac{\sigma_s^2}{2\sigma_t^3} + \frac{(\mu_t - \mu_s)^2}{2\sigma_t^3}. \quad (25)$$

$$(26)$$

Still, either σ_t or σ_s occurs in the denominators as a factor, leading to numerical instability. This proved why we can not use JS or KL divergence for soft alignments in batch normalization.

B Implementation Details

B.1 Detail Parameter Setting

We set the following default parameters:

- $\mathcal{T}_{forget} = 1,000$.
- $\mathcal{T}_{mature} = 200$.
- Augmentation orders in CIFAR10-C, CIFAR100-C and ImageNet-C follow [Yuan *et al.*, 2023].
- In Dirichlet sampling for CIFAR10-C and CIFAR100-C, we choose the number of time slots as same as the number of classes and $\delta = 0.1$. Detail implementation is shown in sec. B.2
- The severity is 5 for all corruption types.
- A fix random seed = 1 for all experiments .

We run all experiments on one V100 GPU.

B.2 Correlation Sampling

Dirichlet Sampling in CIFAR10-C/100-C Traditional test-time adaptation assumes independent identical distributed (i.i.d) test samples, while the test samples might be highly correlated and thus be non-i.i.d. We follow [Yuan *et al.*, 2023] in correlation sampling setting in CIFAR10-C and CIFAR100-C tasks. For each corruption type, we set K time slots. We assume each time slot given a class satisfies a categorical distribution $Cat(\pi)$ which approximately satisfies a Dirichlet distribution $Dir(\delta, \delta, \dots, \delta)$,

$$\pi \sim Dir(\delta, \delta, \dots, \delta), \quad (27)$$

$$p(T = k|y = c) \sim Cat(\pi), \quad (28)$$

where $p(T = k|y = c)$ represents the probability of sample belonging to time slot k given class c , and T denotes the time slot variable. After ensuring $p(T|y)$ for each time slot and each class, we randomly samples of each class to each time slot according to $p(T|y)$. Finally, we shuffle the samples at each time slot. In this way, we mimic the temporal correlation at different time slots. In the experiment, we set the number of time slots K equal to the number of classes C and $\delta = 0.1$.

Notice that, if δ is large, then $p(T = k|y = c) \sim Cat(\pi) \approx Cat(\frac{1}{C}, \frac{1}{C}, \dots, \frac{1}{C})$. In such a scenario, each class is evenly distributed in each time slot, degenerating to i.i.d. test samples. If δ is small, then $p(T = k|y = c) \sim Cat(\pi)$ is highly imbalanced, and the temporal correlation can thus be simulated.

Correlated Sampling in ImageNet-C Each class contains only five samples in each corruption type, making Dirichlet sampling unavailable for correlation simulation. We thus follow [Gong *et al.*, 2022] to sort the ImageNet-C by the labels to simulate correlation. Specifically, the test samples are arranged by their labels and samples in each class will consecutively appear at inference.

C Extra Experiment Results

This section reports parameter analysis on the ν_b, ν_m , and learning rate. For each parameter, we calculate the average classification error across the CIFAR10-to-CIFAR10-C,

the CIFAR100-to-CIFAR100-C, and ImageNet-to-ImageNet-C tasks over 15 corruption types with severity 5 using the default corruption order and correlation sampling methods.

We first explore the influence from ν_b by running experiments with ν_b in [0.001, 0.005, 0.01, 0.05, 0.1, 0.5]. ν_b represents the extent to which the global target statistics are updated. Low ν_b exhibits large performance declines as the target statistics are almost unchanged and the model suffers from domain shifts. High ν_b shows relatively smaller performance declines.

Table 8: **Parameter analysis on ν_b .** Average classification error (%).

ν_b	CIFAR10-C	CIFAR100-C	ImageNet-C
0.001	36.6	56.2	80.7
0.005	28.6	40.6	76.2
0.01	25.2	35.4	73.1
0.05	22.4	33.5	66.7
0.1	23.7	34.3	66.9
0.5	28.3	35.6	68.8

Next, we investigate the impact of ν_m by using a range [0.0001, 0.0005, 0.001, 0.005, 0.01, 0.05]. ν_m represents how fast the teacher model is updated. Large ν_m results in a significant performance degradation. For instance, the average class error increases from 22.4 % to 38.1 % in the CIFAR10-C task when raising ν_m from 0.001 to 0.05. However, the model is non-sensitive to lower ν_m .

Table 9: **Parameter analysis on ν_m .** Average classification error (%).

ν_m	CIFAR10-C	CIFAR100-C	ImageNet-C
0.0001	24.2	34.9	69.8
0.0005	22.7	33.6	68.0
0.001	22.4	33.5	66.7
0.005	27.1	38.0	70.6
0.01	30.7	41.0	78.8
0.05	38.1	48.8	94.1

Lastly, we study the sensitivity of the learning rate in the range of [5×10^{-5} , 0.0001, 0.0005, 0.001, 0.005, 0.01]. The model performance is stable when varying the learning rate. Nevertheless, too large learning rates lead to model performance collapse in the ImageNet-C task.

Table 10: **Parameter analysis on the learning rate.** Average classification error (%).

learning rate	CIFAR10-C	CIFAR100-C	ImageNet-C
5×10^{-5}	25.4	34.3	68.7
0.0001	25.3	34.0	68.3
0.0005	22.7	33.7	67.5
0.001	22.4	33.5	66.7
0.005	22.9	34.1	66.5
0.01	23.5	40.3	95.1